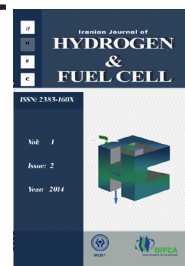


Iranian Journal of Hydrogen & Fuel Cell

IJHFC

Journal homepage://ijhfc.irost.ir



Synthesis, characterization and hydrogen storage properties of $Mm(Ni, Co, Mn, Al)_5$ alloy

Seyyed Mojtaba Alavi Sadr (Zareii)¹, Hadi Arabi^{2,*}, Faiz Pourarian³

¹ Magnetism and Superconducting Research Laboratory, Department of Physics, Faculty of Science, University of Birjand, Birjand, Iran

² Department of Physics, Faculty of Science, Ferdowsi University of Mashhad, Mashhad, Iran

³ Department of Material Science and Engineering, Carnegie Mellon University, Pittsburgh, PA, USA

Article Information

Article History:

Received:

11 February 2014

Received in revised form:

14 July 2014

Accepted:

6 September 2014

Keywords

Hydrogen storage

$Mm(Ni, Co, Mn, Al)_5$ alloy

Structural properties

Pressure-composition isotherm

Hydriding kinetic

Abstract

This paper investigates hydrogenation characterizations and effect of hydrogenation/dehydrogenation (H/D) cycling on the structural and morphological properties of $MmNi_{4.22}Co_{0.48}Mn_{0.15}Al_{0.15}$ (Mm=mischmetal) alloy. The alloy was prepared by arc melting method and it was re-melted several times under argon atmosphere. The results indicate that after several H/D cycles, the alloy is pulverized into fine particles, however, it keeps its hexagonal $LaNi_5$ -type structure. The pressure-composition isotherms of H/D reactions and absorption kinetics were measured in the temperature range 293-338K. The absorption plateau pressures were determined to be ~0.51, 1.22 and 2.49 bar at 293, 313 and 333K respectively, with a maximum hydrogen storage capacity of about 5.78 at 293K. The enthalpy (ΔH), entropy (ΔS) and the activation energy of reactions (E_a) were also calculated. The results show the hydrogenation reaction rate increases with an increase in the operating temperature or pressure. The Jander diffusion (JDM) and Johnson-Mehl-Avrami (JMA) models were employed and the kinetic of hydrogenation was analyzed in detail for hydriding reaction (rate controlling steps) mechanism. The results indicate that the $MmNi_{4.22}Co_{0.48}Mn_{0.15}Al_{0.15}$ alloy has potential for use in practical applications.

1. Introduction

The problems of energy shortage and environmental contamination encourage using sustainable and clean energy sources [1]. Hydrogen as a clean fuel is an excellent energy carrier to be used in both fuel cells and internal combustion engines [1]. However, hydrogen storage is the fundamental key challenge towards the hydrogen economy [1,2]. Amongst the

conventional hydrogen storage methods, metal hydrides are the promising candidates due to their safety advantage along with high volume efficient storage capacity for on-board applications [3]. In the metal hydrides family, $LaNi_5$ -based alloys have been found to be very attractive due to their significant quantities of hydrogen storage capacity, fast and reversible sorption properties and plateau pressure of a few bars at room temperature [4]. However, besides

*Corresponding author Email: Department of Physics, Ferdowsi University of Mashhad, P.O.Box: 9177948974, Mashhad, Iran.
Tel: 051-38796416, Fax: 051-38796983, E-mail: arabi-h@um.ac.ir

the high cost of raw materials, they have some unsatisfactory properties such as the disproportionation problem and easy pulverization after several hydrogen (absorption/desorption) cycles [4, 5]. In the disproportionation process occurring during cycling, the alloy decomposes into more thermodynamically stable decomposition products [5]. In this context, many attempts have been made which indicate that the substitution of some amount of nickel in these materials with other metals such as Al, Co and Mn while LaNi_5 -type crystal structure of alloys remaining the same, can improve some of their hydrogen storage and electrochemical characteristics [4,6-11]. The partial substitution of Co for Ni in LaNi_5 is effective in reducing the plateau pressure and improving the cycling stability of the alloy during hydriding process [6]. On the other hand, a partial substitution of Ni by Al can improve the cycling performance and absorption kinetics, and decrease the plateau pressure, but it impairs the hydrogen storage capability to some extent [7]; meanwhile, Mn substitution can decrease the plateau pressure of the hydride without reducing the hydrogen content, although the hydride hysteresis factor slightly increases [7]. Furthermore, using a combination of rare earth elements (Mm= mischmetal) including La, Ce, Pr and Nd in place of La can reduce the initial cost [12]. Although these methods are used as some of the most effective techniques to enhance the overall hydrogen storage properties of hydrides, the results are not still completely satisfactory [11,13]. The hydrogen experiments indicated that $\text{Mm}(\text{Ni},\text{Co},\text{Mn},\text{Al})_5$ alloys appear to be a promising materials for practical applications [14,15].

In this work, the structural, morphological and hydrogen storage characterizations of $\text{MmNi}_{4.22}\text{Co}_{0.48}\text{Mn}_{0.15}\text{Al}_{0.15}$ alloy are investigated in detail, and the results are discussed. The Jander diffusion (JDM) and Johnson-Mehl-Avrami (JMA) models were also employed for the kinetic analysis of hydriding reaction. To the best of our knowledge, there is no report on the synthesis, hydrogen storage and different physical properties of this alloy. The elemental ratio of 4.22/0.48/0.15/0.15 for

Ni/Co/Mn/Al, respectively are particularly selected to make the alloy suitable for hydrogenation (control hydride stability) with working practical pressures below 1.0 MPa and temperatures in the range from 253 to 373K.

2. Experimental details

2.1. Synthesis of the alloy

The stoichiometric $\text{MmNi}_{4.22}\text{Co}_{0.48}\text{Mn}_{0.15}\text{Al}_{0.15}$ alloy (Mm consisted of 48.62 wt% La, 2.04 wt% Ce, 9.85 wt% Pr and 39.49 wt% Nd) was prepared in an arc furnace under high purity argon atmosphere on a water-cooled copper hearth. This ingot was turned over and re-melted three times for homogeneity. The purity of raw materials was more than 99.9%. The ingot was then annealed in a sealed evacuated quartz tube for one week at 1373K and subsequently rapidly cooled to obtain a single-phase sample.

2.2. Characterization details

The structural analyses of samples including their X-ray diffraction (XRD) powder patterns, before and after 30 hydrogenation/dehydrogenation (H/D) cycles, were examined by means of X'Pert Pro, PANalytical system (Cu-K α : $\lambda = 1.540598\text{\AA}$) at room temperature. To investigate their microstructural properties, the scanning electron microscope linked with an energy dispersive X-ray spectrometer (SEM-EDS, model VEGA/TESCAN) was employed. The hydrogen absorption/desorption behaviors of the alloy were measured by using a volumetric gas absorption (Sievert) apparatus installed in our laboratory [2]. The validation and calibration of the Sievert apparatus was performed by using the standard alloy LaNi_5 . This sample was hydrogenated and the hydrogen storage capacities and pressure-composition (PC) isotherms were measured at different temperatures. This procedure was repeated several times. The results, after calibration of the unit were found to be in excellent agreement with reputable literature [16].

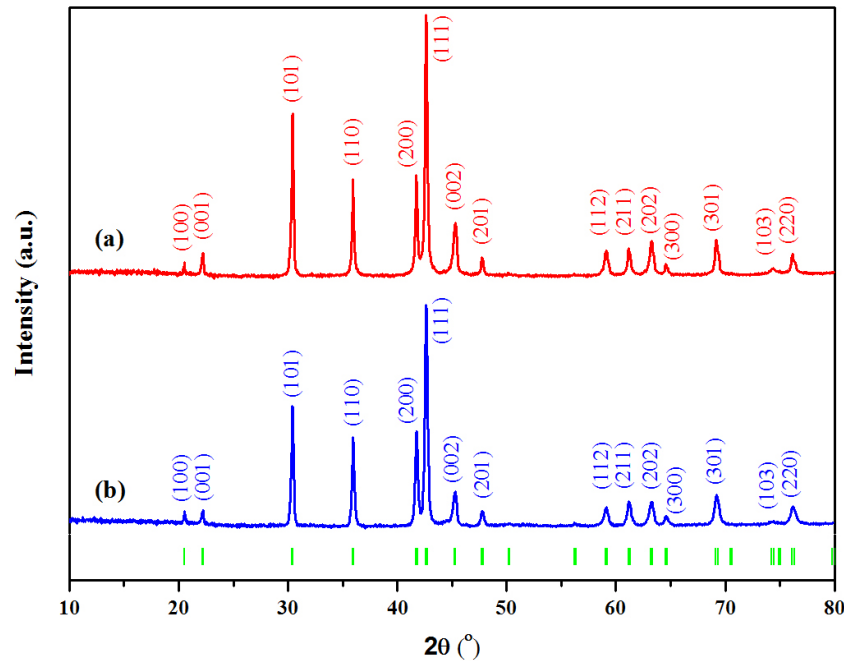


Fig. 1. XRD profiles of $\text{MmNi}_{4.22}\text{Co}_{0.48}\text{Mn}_{0.15}\text{Al}_{0.15}$ alloy (a) before hydrogen activation; (b) after 30 H/D cycles.

Then, the hydrogen storage capacities and PC isotherms of $\text{MmNi}_{4.22}\text{Co}_{0.48}\text{Mn}_{0.15}\text{Al}_{0.15}$ alloy at different temperatures were measured.

2.3. Materials and techniques

For XRD measurements of the non-cycled $\text{MmNi}_{4.22}\text{Co}_{0.48}\text{Mn}_{0.15}\text{Al}_{0.15}$ alloy, fractions of the as-annealed ingot were pulverized in an agate mortar to fine particles (sample A_1) under argon atmosphere in a glove box. The fine powders cause a good signal to noise (S/N) ratio, avoid fluctuation in intensity and spottiness, randomize orientation and also ensure enough particle participation during XRD measurements [17,18]. For hydrogenation measurements, the ingot of the annealed $\text{MmNi}_{4.22}\text{Co}_{0.48}\text{Mn}_{0.15}\text{Al}_{0.15}$ alloy was crushed to smaller pieces (sample A_2) and introduced into the stainless-steel reactor. The sample was first activated [5] through several H/D cycles under 4000kPa initial supply pressure of H_2 gas at 313K. The dehydrogenation process was done by heating the sample to 673K under vacuum of about 1 Pa. When the sample was completely activated, the PC isotherms and kinetics behaviors of the hydrogenation reaction at different temperatures were studied. The

detailed experimental procedure to collect these data has been described in Ref. 5. After 30 H/D cycles, hydrogen gas was completely desorbed by sample A_3 . Finally, in order to reveal the effect of H/D cycling on the structural and microstructural properties of $\text{MmNi}_{4.22}\text{Co}_{0.48}\text{Mn}_{0.15}\text{Al}_{0.15}$ alloy, the dehydrogenated sample was also characterized by XRD and SEM.

3. Results and discussion

3.1. X-ray and microstructure characterizations

Fig. 1(a, b) shows XRD profiles of the non-cycled and cycled alloy. The results indicate that this alloy, both before and after H/D cycling, is a homogeneous single phase and all the peaks are assigned to the hexagonal LaNi_5 -type structure (with space group: $P6/mmm$; JCPDS/PDF No.: 98-008-9646). After 30 H/D cycles, no trace of the disproportionation process is observed in the alloy, while we observed it in LaNi_5 system [2]. This reveals that the cycling stability of this alloy is better than that of LaNi_5 .

Table 1 presents the results of XRD analysis using X'Pert HighScore Plus software. This table lists the

values of lattice parameters, unit cell volumes, overall broadening at half maximum (FWHM) of the main peak (111), average crystallite size (D_{avg}) and lattice strain (ϵ %) of the samples.

Table 1. Structural parameters, FWHM (111), average crystallite size and microstrain of the non-cycled and cycled samples.

Sample	Lattice parameters		Volume $V[\text{\AA}^3]$	FWHM (111) [$^\circ$]	D_{avg} [nm]	$\epsilon\%$
	a [\AA]	c [\AA]				
Non-cycled sample	4.9962	4.0048	86.575	0.194	160	0.097
Cycled sample	4.9954	4.0079	86.614	0.252	124	0.113

As seen, compared with the alloy before cycling, the lattice constants a and c slightly decreased and increased after cycling, respectively. Such behavior was also observed for other LaNi_5 -based hydride alloys [2,19-20] which suggests that the metal atoms should be rearranged with the formation of lattice defects (vacancy and dislocation) during H/D process [21]. After cycling, FWHM increases indicating that the H/D cycling causes the peaks to be slightly broadened. This can be due to the lattice strain generated during H/D cycling, and reduction in crystallite size (Table 1) [22, 23]. The peak broadening effects caused by crystallite size and microstrain were separated by Williamson-Hall (W-H) method [2]. In these calculations, the contribution of peak broadening

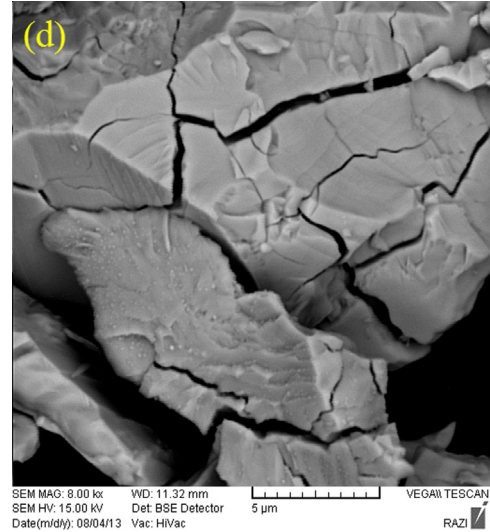
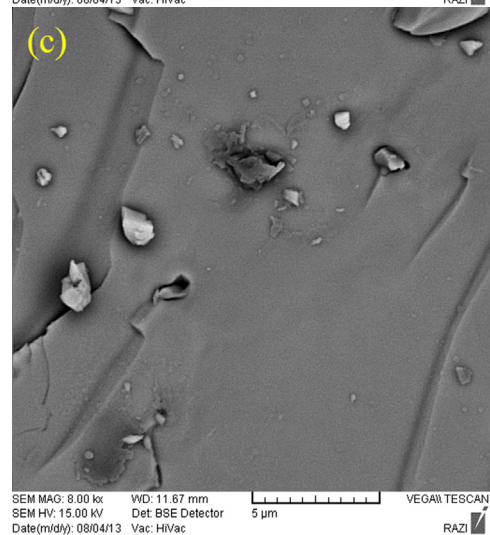
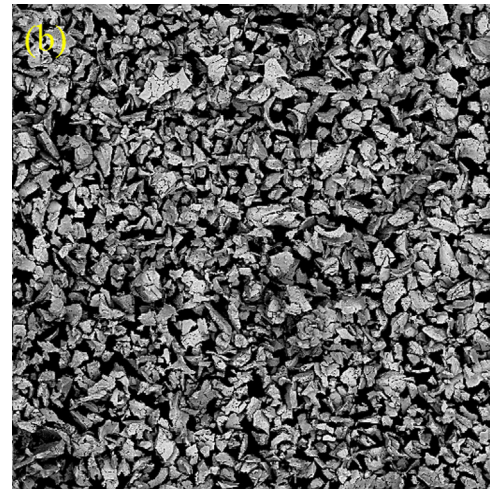


Fig. 2. SEM images of (a and c) alloy ingots put in the reactor before hydrogenation; (b and d) the alloy after selected 30 H/D cycles.

arising from the instrument was considered by using XRD profile of a pure Si sample. Using W-H method, the values of average crystallites size for the non-cycled and dehydrogenated alloy $\text{MmNi}_{4.22}\text{Co}_{0.48}\text{Mn}_{0.15}\text{Al}_{0.15}$ are estimated to be about 160 nm and 124 nm respectively (Table 1). This means that the hydrogen absorption/desorption process leads to alloy pulverization as will be confirmed later by SEM results (see Figure 2).

Fig. 3 shows the SEM images of the powders analyzed by XRD (sample A₁) at two different magnifications. The size distribution of particles is mostly less than 5 μm , although some larger particles within a range of 7-20 μm can still be seen. Furthermore, the results of

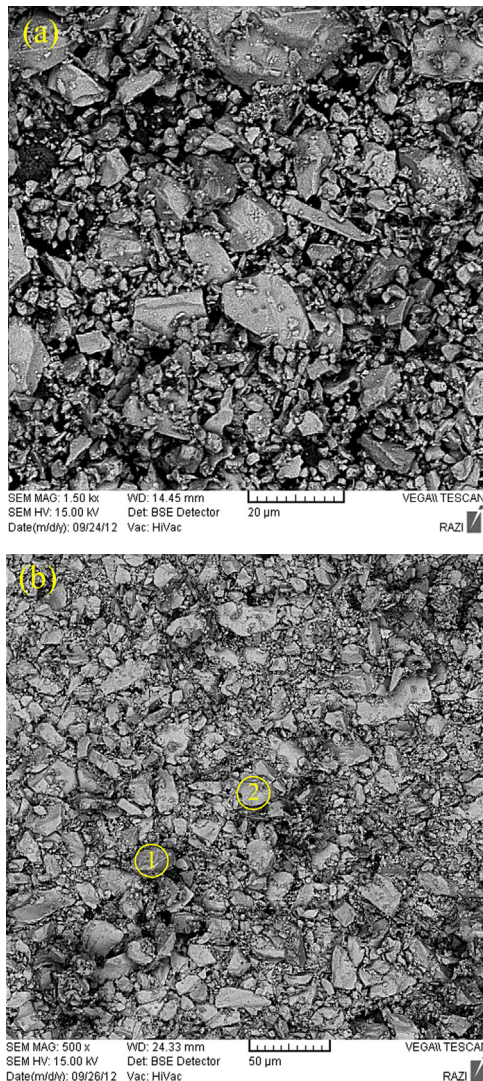


Fig. 3. SEM images of $\text{MmNi}_{4.22}\text{Co}_{0.48}\text{Mn}_{0.15}\text{Al}_{0.15}$ alloy powder. The circles with solid line indicate the areas of (1) and (2).

EDS analysis, for areas of 1 and 2 indicated as circles with solid line in Fig. 3b, are presented in Table 2. The

Table 2. EDS results (in weight) of $\text{MmNi}_{4.22}\text{Co}_{0.48}\text{Mn}_{0.15}\text{Al}_{0.15}$ alloy powder.

Area	%Weight							
	La	Ce	Pr	Nd	Ni	Co	Mn	Al
1	14.92	0.83	2.74	11.60	60.76	6.15	2.10	0.90
2	14.12	0.76	2.77	12.50	60.83	5.97	1.98	1.07

EDS results show that areas 1 and 2 have nearly similar elemental composition corresponding to chemical composition of $\text{La}_{0.45}\text{Ce}_{0.02}\text{Nd}_{0.34}\text{Pr}_{0.08}\text{Ni}_{4.36}\text{Co}_{0.44}\text{Mn}_{0.16}\text{Al}_{0.14}$ and $\text{La}_{0.43}\text{Ce}_{0.02}\text{Nd}_{0.36}\text{Pr}_{0.08}\text{Ni}_{4.36}\text{Co}_{0.43}\text{Mn}_{0.15}\text{Al}_{0.17}$. To clarify the effect of hydrogen absorption/desorption on the microstructure of the alloy, the SEM images of non-cycled ingots put in the reactor and that of cycled sample after 30 H/D cycles were taken and shown in Fig. 2(a-d). As seen, after H/D cycling the size of particles significantly decreases, with a nearly uniform size distribution compared to non-cycled ones. This means that the hydrogen absorption/desorption pulverizes the alloy into fine particles, in agreement with XRD results. Actually, the internal stress created in the lattice structure due to the volume expansion (shrinkage) from hydrogen absorption (desorption) is the driving force that pulverizes the alloy [14, 20]. On the other hand, no crack was observed on the surface of non-cycled particles (Fig. 2 (a), (c)), while some cracks were developed after H/D cycling (Fig. 2 (b), (d)). Formation of new small particles and hence pulverization of the alloy might have resulted from propagations of these microcracks. This indicates that cracking and pulverization, during H/D cycling, might take place simultaneously [20].

3.2. Hydrogenation behavior

3.2.1. PC isotherms

One of the most important material characteristics for a metal hydride is PC isotherm curves [24]. The absorption and desorption PC isotherms of activated $\text{MmNi}_{4.22}\text{Co}_{0.48}\text{Mn}_{0.15}\text{Al}_{0.15}$ alloy at 293, 313 and 333K

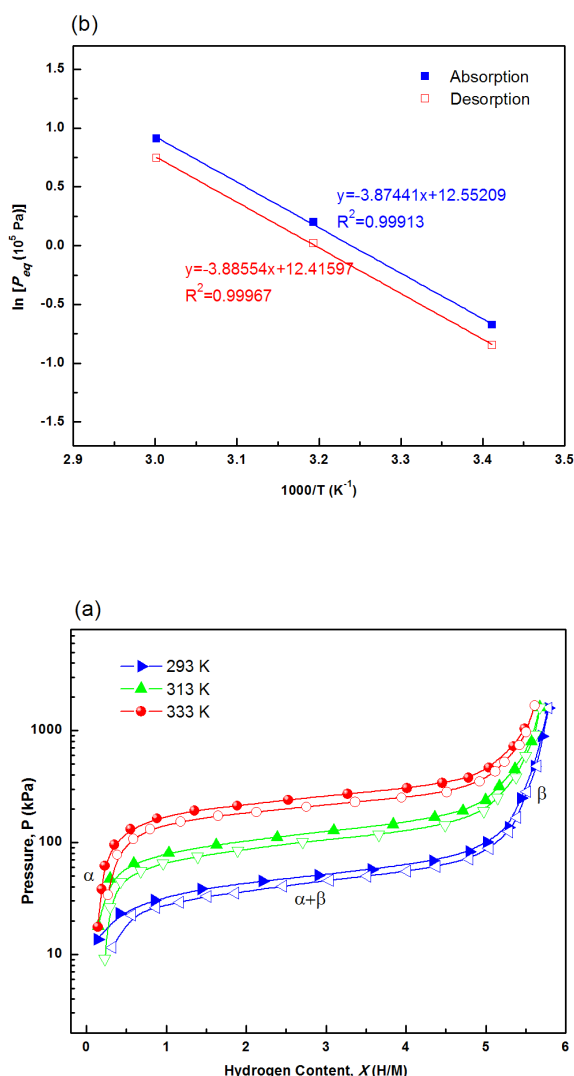


Fig. 4. (a) PC isotherms; (b) Van't Hoff plots of the hydrogen absorption (filled symbols) and desorption (empty symbols) for $\text{MmNi}_{4.22}\text{Co}_{0.48}\text{Mn}_{0.15}\text{Al}_{0.15}\text{-H}$ system.

are shown in Fig. 4a. The hydrogen capacity X is defined as the hydrogen-to-metal atomic ratio H/M (M

= represents alloys or compound metal) [5]. There are two single-phase regions (α and β) and one dual-phase region ($\alpha + \beta$) in PC isotherms of the alloy. Table 3 presents the values of maximum hydrogen capacity, absorption and desorption equilibrium pressures at the mid-point of the plateau region (P_{eq}^{abs} and P_{eq}^{des}) and hysteresis loss which is calculated from $\frac{1}{2}RT \ln(P_{eq}^{abs} / P_{eq}^{des})$. The maximum hydrogen storage capacity of about 5.78 (i.e. $\text{MmNi}_{4.22}\text{Co}_{0.48}\text{Mn}_{0.15}\text{Al}_{0.15}\text{H}_{5.78}$) was obtained at $T = 293\text{K}$ under equilibrium pressure $\sim 1600\text{kPa}$, which is higher than that of $\text{MmNi}_{4.3-x}\text{Co}_x\text{Mn}_{0.33}\text{Al}_{0.4}$ ($H/M \sim 5.24$ at 293K) [25], $\text{MmNi}_{3.55}\text{Co}_{0.75}\text{Mn}_{0.4}\text{Al}_{0.3}$ ($H/M \sim 5.4$ at 293K) [26], $\text{MmNi}_{3.6}\text{Co}_{0.85}\text{Mn}_{0.4}\text{Al}_{0.15}$ ($H/M \sim 5.2$ at 318K) [11], but less than that for LaNi_5 ($H/M \sim 6$ at 296K) [27]. Moreover, the reversible hydrogen storage capacity or plateau width for this alloy was found to be ~ 4.1 at 293K , larger than that of $\text{MmNi}_{3.55}\text{Co}_{0.75}\text{Mn}_{0.4}\text{Al}_{0.3}$ (~ 3.3) [26] and $\text{MmNi}_{3.6}\text{Co}_{0.85}\text{Mn}_{0.4}\text{Al}_{0.15}$ (~ 3.2) [11], but lower than that of alloy LaNi_5 (~ 5.6) [28], under the same conditions. As seen, the hydrogen capacity decreases with temperature, while the values of plateau pressures significantly increase. It is found that the variation of the hydrogen absorption and desorption plateau pressure (10^5 Pa) with temperature (K) follow $\ln P_{eq}^{abs} = -3874.41/T + 12.5521$ and $\ln P_{eq}^{des} = -3885.54/T + 12.4160$ relations, respectively (Fig. 4b).

In fact, with an increase in temperature, more hydrogen gas is desorbed during the hydrogen absorption that resulted in decreasing the amount of hydrogen capacity and increasing the equilibrium pressures [29]. With increasing the temperature to 313K , the hysteresis loss increases and then with further increase in temperature, it decreases. This behavior was also observed for other LaNi_5 -based alloys [14, 30-31].

The enthalpy (ΔH) and entropy (ΔS) of H/D

Table 3. The maximum hydrogen content (H/M), mid-absorption and desorption plateau pressures and hysteresis loss of $\text{MmNi}_{4.22}\text{Co}_{0.48}\text{Mn}_{0.15}\text{Al}_{0.15}$ hydride at different temperatures.

T (K)	H/M	P_{eq}^{abs} ($\times 10^5\text{ Pa}$)	P_{eq}^{des} ($\times 10^5\text{ Pa}$)	Hysteresis loss (kJ/mol)
293	5.78	0.51	0.43	0.21
313	5.67	1.22	1.02	0.233
333	5.61	2.49	2.11	0.229

process were evaluated from PC isotherms using the Van't Hoff plot method [32] shown in Fig. 4b. The values of ΔH and ΔS of hydrogen absorption (desorption) reaction for the alloy were estimated to be $\sim -32.21 \pm 0.67$ ($+32.31 \pm 0.41$) J/mol $H_2 \cdot K^{-1}$ and -104.37 ± 2.15 (-103.23 ± 1.32) kJ/mol H_2 , respectively. These differences are a consequence of the hysteresis effect [33]. The estimated enthalpy for the hydride formation of investigated alloy is found to be more negative than that of $LaNi_5$ (-27.76 kJ/mol H_2 [34]) implying more thermodynamic stability of $MmNi_{4.22}Co_{0.48}Mn_{0.15}Al_{0.15}$ alloy compared to $LaNi_5$. It has been suggested that for practical applications, the heat of alloy hydride formation should be between -40 and -15 kJ/mol [35]. In case it is more positive than -15 kJ/mol, the alloy hydride is not stable enough for hydriding at room temperature. On the other hand, the hydrides that are too stable make dehydrogenation very difficult. As concluded, the values of the equilibrium pressures and hence enthalpy of hydriding reaction of $MmNi_{4.22}Co_{0.48}Mn_{0.15}Al_{0.15}$ alloy fall within an appropriate range to make it suitable for practical applications.

3.2.2. Hydrogen absorption kinetics

A hydrogen storage device is also characterized by its storage capacity and the rate at which it stores or releases the hydrogen [36, 37]. Accordingly, the hydriding kinetic measurements of $MmNi_{4.22}Co_{0.48}Mn_{0.15}Al_{0.15}$ alloy were carried out within two schemes: (i) absorption kinetic at constant temperature (314K) under different initial supply pressures of storage cell (Fig. 5), and (ii) absorption kinetic at different temperatures by keeping the driving pressure ratio (P_r) equal to 4 for all experiments (Fig. 6a).

As seen, the hydrogen content X significantly increases with an increment in hydrogen applied pressure: 2.26, 4.10, 4.93, 5.43 and 5.70 for 600, 1000, 1300, 1800 and 3600 kPa hydrogen pressures, respectively. Furthermore, the characteristic reaction time ($t_{0.9}$), which is shown on the figure and is the required time that sample reaches 90% of maximum hydrogen capacity, becomes smaller. This means

that the hydriding reaction rate becomes faster with pressure.

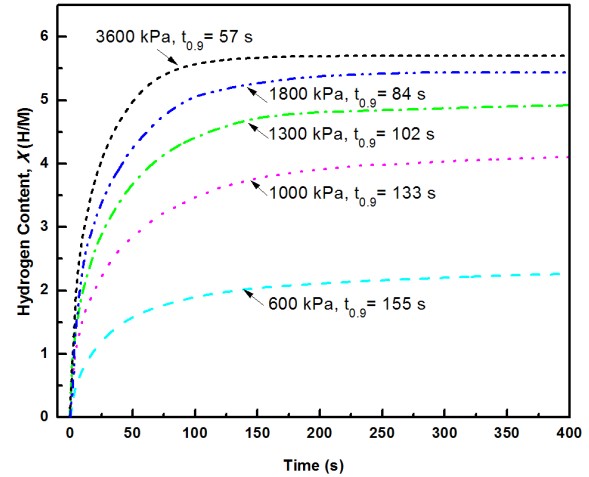


Fig. 5. The hydriding kinetic plots of $MmNi_{4.22}Co_{0.48}Mn_{0.15}Al_{0.15}$ alloy at 314K under different initial supply pressures.

At a given temperature, the main driving force of the hydrogen absorption for a hydrogen storage media is the initial hydrogen pressure. So the increase of the initial pressure during the hydriding reaction means the increase of hydrogen concentration in the surface of the sample. In other words, the driving force which diffuses the H atoms into the bulk of sample increases with increasing of initial pressure [36]. This is why the hydrogen capacity and reaction rate increase with pressure. On the other hand, because of the larger difference between applied and hydride equilibrium pressures the absorption rate is high at the beginning and gradually decelerates and approaches to zero at the end of the process.

The influence of operating temperature ($T = 293, 314$ and $338K$) on the hydrogen absorption kinetics of the alloy under a constant driving pressure ratio ($P_r = 4$) is shown in Fig. 6a. The pressure ratio was defined as ratio of gas pressure to equilibrium pressure [38]. The equilibrium pressure values of the alloy were obtained from PC isotherms.

It can be seen that hydriding reaction rate increases with temperature. Actually, with increasing temperature, more H_2 molecules are dissociated to H atoms [39] which cause the reaction rate to be increased. For analysis of the hydrogen absorption reaction, we

employed different fitting models. Depending on the rate controlling mechanisms, different kinetic models have been proposed in the literature [38, 40-41].

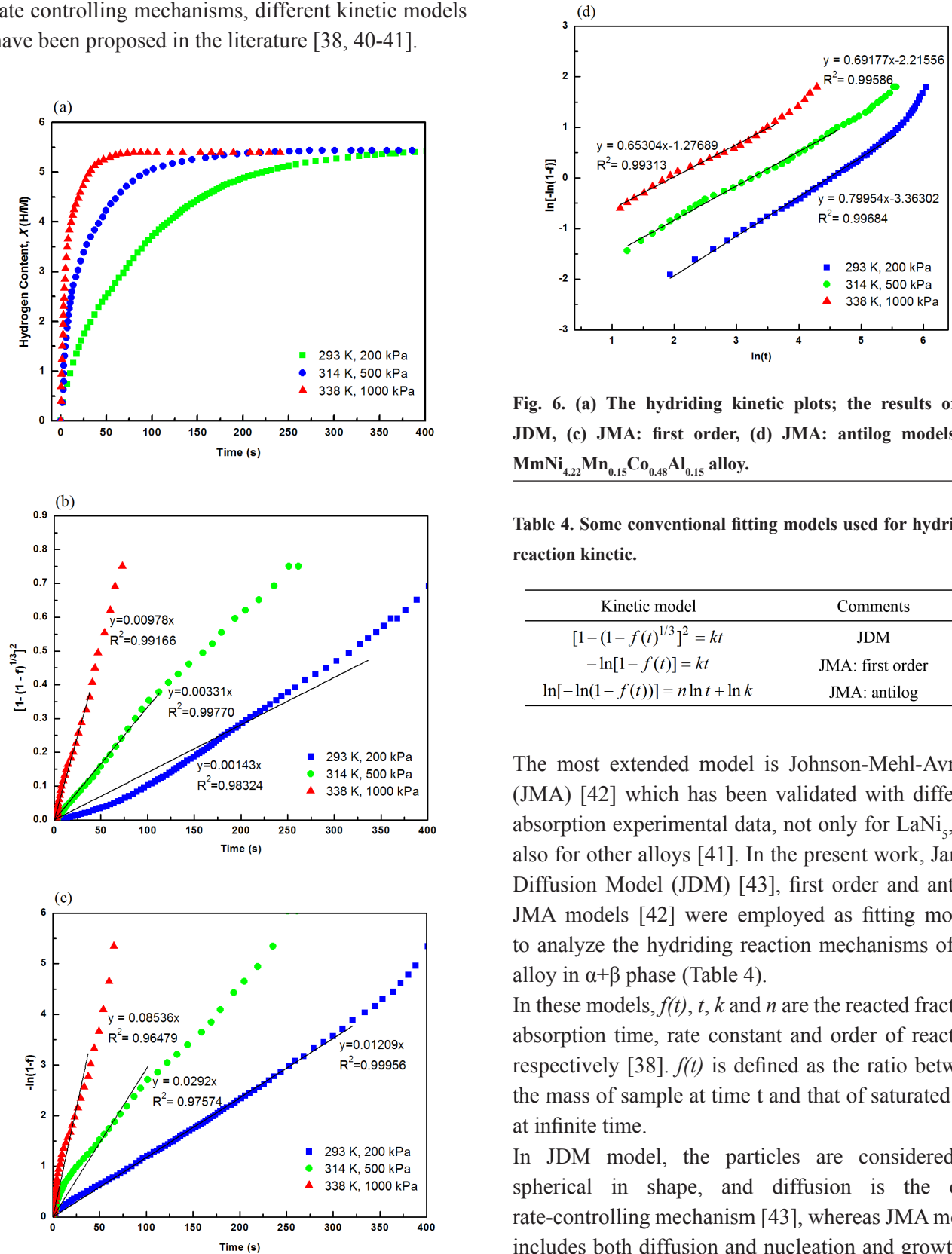


Fig. 6. (a) The hydriding kinetic plots; the results of (b) JDM, (c) JMA: first order, (d) JMA: antilog models for $\text{MmNi}_{4.22}\text{Mn}_{0.15}\text{Co}_{0.48}\text{Al}_{0.15}$ alloy.

Table 4. Some conventional fitting models used for hydriding reaction kinetic.

Kinetic model	Comments
$[1 - (1 - f(t))^{1/3}]^2 = kt$	JDM
$-\ln[1 - f(t)] = kt$	JMA: first order
$\ln[-\ln(1 - f(t))] = n \ln t + \ln k$	JMA: antilog

The most extended model is Johnson-Mehl-Avrami (JMA) [42] which has been validated with different absorption experimental data, not only for LaNi_5 , but also for other alloys [41]. In the present work, Jander Diffusion Model (JDM) [43], first order and antilog JMA models [42] were employed as fitting models to analyze the hydriding reaction mechanisms of the alloy in $\alpha+\beta$ phase (Table 4).

In these models, $f(t)$, t , k and n are the reacted fraction, absorption time, rate constant and order of reaction, respectively [38]. $f(t)$ is defined as the ratio between the mass of sample at time t and that of saturated one at infinite time.

In JDM model, the particles are considered as spherical in shape, and diffusion is the only rate-controlling mechanism [43], whereas JMA model includes both diffusion and nucleation and growth as the rate-controlling mechanisms [41]. From Table 4,

it can be seen that for a constant temperature, plots of $[1 - (1 - f(t))^{1/3}]^2$ and $-\ln(1 - f(t))$ vs. absorption time (t) respectively for JDM and first order JMA models, are the straight lines with slope k . For antilog JMA model, a plot of $\ln \frac{1-f}{t} - f t$ vs. $\ln(t)$ is a straight line with slope n and intersect $\ln(k)$. Fig. 6(b-d) shows the results of JDM, first order and antilog JMA models, respectively. The values of calculated rate constant along with linear regression equations (R^2) are presented in the figures. For JDM model, the derivation of experimental data is rather larger at 314K. Similar to this behavior has been observed for $\text{La}(\text{Ni},\text{Al})_5$ alloy by Muthukumar et al. [38]. The results indicate that the values of linear regression equations (R^2) at 293, 314 and 338K are highest for the first order JMA, JDM and antilog JMA models, respectively. Therefore, we can conclude that the rate-controlling step at 314K is diffusion, while the diffusion along with nucleation and growth are the rate-controlling steps at 298 and 338K. Similar behavior has been reported for other LaNi_5 -based alloy [38]. However, all three models confirm that the rate constant and hence the reaction rate increase with temperature. Then, by using the calculated values of rate constant k , the activation energy E_a of hydrogen absorption reaction was evaluated by Arrhenius relationship:

$$k = A \exp(-E_a/RT) \quad (1)$$

where A and R are the pre-exponential factor and universal gas constant, respectively [38]. A plot of $\ln(k)$ vs. $1/T$ is a straight line with slope $-E_a/R$. The values of E_a are estimated to be about 35.17, 35.76 and 37.26 kJ/mol H_2 using JDM, first order and antilog JMA models respectively. These results are also close to activation energy of MmNi_5 alloy, 35.7 kJ/mol H_2 [44].

4. Conclusions

In this work, the structural and morphological properties of a newly developed

$\text{MmNi}_{4.22}\text{Co}_{0.48}\text{Mn}_{0.15}\text{Al}_{0.15}$ alloy were studied before and after 30 hydrogenation /dehydrogenation (H/D) cycles. Although after cycling the diffraction peaks were slightly broadened, hexagonal LaNi_5 -type structure of the alloy was maintained, without trace of the disproportionation process. SEM images confirmed that H/D cycling pulverizes the alloy ingot into fine particles. The pressure-composition isotherms of hydrogen absorption/desorption were determined in the temperature range of 293-333K, and the values of enthalpy and entropy of hydrogen absorption (desorption) were evaluated to be about -32.21 (+32.31) kJ/mol H_2 and -104.37 (-103.23) J/mol $\text{H}_2\cdot\text{K}^{-1}$ respectively. The hydriding kinetic measurements showed that the hydrogen storage capacity of the alloy increases with the applied pressure at constant temperature. Moreover, the rate of hydriding reaction increases with temperature under a constant driving pressure ratio of H_2 gas. The hydriding kinetic mechanism of the alloy was clarified using JDM and JMA (first order and antilog) models. The results indicated that diffusion along with nucleation and growth are the rate-controlling steps for the hydriding reaction at 293 and 338K, while the rate-controlling step at 314K is diffusion. The activation energy of the hydride alloy is calculated to be about 35.17, 35.76 and 37.26 kJ/mol H_2 by JDM, first order JMA and antilog JMA models, respectively.

Acknowledgments

The authors would like to thank the Renewable Energy Organization of Iran (SUNA) for their financial support.

5. References

1. Zareii S. M. and Sarhaddi R., "Structural, electronic properties and heat of formation of Mg_2FeH_6 complex hydride: an ab initio study", Phys. Scr., 2012, 86: 015701.

2. Zareii (Alavi Sadr) S. M., Arabi H., Pourarian F. and Sarhaddi R., "Physical properties and electronic structure of LaNi_5 compound before and after hydrogenation: An experimental and theoretical approach", *Iran. J. Hydrogen Fuel Cell*, 2014, 1: 27.
3. Sakintuna B., Lamari-Darkrim F. and Hirscher M., "Metal hydride materials for solid hydrogen storage: A review", *Int. J. Hydrogen Energy*, 2007, 32: 1121.
4. Xie J-y. and Chen N-x., "Site preference and structural transition of $\text{R}(\text{Ni}, \text{M})_5$ ($\text{R}=\text{La}, \text{Nd}, \text{Gd}$), ($\text{M}=\text{Al}, \text{Fe}, \text{Co}, \text{Cu}, \text{Mn}$)", *J. Alloys Compd.*, 2004, 381: 1.
5. Broom D. P., *Hydrogen Storage Materials, Green Energy and Technology*, Springer-Verlag, 2011.
6. Asano K., Yamazaki Y. and Iijima Y., "Hydriding and dehydriding processes of $\text{LaNi}_{5-x}\text{Co}_x$ ($x= 0-2$) alloys under hydrogen pressure of 1-5 MPa", *Intermetallics*, 2003, 11: 911.
7. Li S. L., Wang P., Chen W., Luo G., Han X. B., Chen D. M. and Yang K., "Study on hydrogen storage properties of $\text{LaNi}_{3.8}\text{Al}_{1.2-x}\text{Mn}_x$ alloys", *Int. J. Hydrogen Energy*, 2010, 35: 12391.
8. Mungole M. N. and Balasubramaniam R., "Hydrogen desorption kinetics in $\text{MmNi}_{4.2}\text{Al}_{0.8}\text{-H}$ system", *Int. J. Hydrogen Energy*, 1998, 23: 349.
9. Mungole M. N., Balasubramaniam R., Rai K. N., "Magnetization behavior of hydrogen storage MmNi_5 intermetallics with Al, Mn and Sn substitutions", *Int. J. Hydrogen Energy*, 1997, 22: 679.
10. Ayari M., Paul-Boncour V., Lamloumi J., Mathlouthi H. and Percheron-Guégan A., "Study of the structural, thermodynamic and electrochemical properties of $\text{LaNi}_{3.55}\text{Mn}_{0.4}\text{Al}_{0.3}(\text{Co}_{1-x}\text{Fe}_x)_{0.75}$ ($0 \leq x \leq 1$) compounds used as negative electrode in Ni-MH batteries", *J. Alloys Compd.*, 2006, 420: 251.
11. Ma J., Pan H., Chen C. and Wang Q., "Effect of heat treatment on the microstructure and electrochemical properties of AB_5 -type $\text{MmNi}_{3.60}\text{Co}_{0.85}\text{Mn}_{0.40}\text{Al}_{0.15}$ hydride alloy: 1.-The microstructure and P-C isotherms, *Int. J. Hydrogen Energy*, 2002, 27: 57.
12. Jain I. P., Abu Dakka M. I. S and Vijay Y.K., "Hydrogen absorption in Al doped MmNi_5 ", *Int. J. Hydrogen Energy*, 2000, 25: 663.
13. Yang S., Han S., Li Y., Yang S. and Hu L., "Effect of substituting B for Ni on electrochemical kinetic properties of AB_5 -type hydrogen storage alloys for high-power nickel/metal hydride batteries", *Mater. Sci. Eng. B*, 2011, 176: 231.
14. Li S. L., Chen W., Chen D. M. and Yang K., "Effect of long-term hydrogen absorption/desorption cycling on hydrogen storage properties of $\text{MmNi}_{3.55}\text{C}_{0.75}\text{Mn}_{0.4}\text{Al}_{0.3}$ ", *J. Alloys Compd.*, 2009, 474: 164.
15. Ayari M., Boncour V. P., Lamloumi J. and Guegan A. P., "Magnetic properties of $\text{LaNi}_{3.55}\text{Mn}_{0.4}\text{Al}_{0.3}\text{Co}_{0.75-x}\text{Fe}_x$ ($x=0; 0.35$) compounds before and after electrochemical cycles", *J. Magn. Magn. Mater.* 2002, 242-245: 850.
16. Senoh H., Takeichi N., Takeshita H. T., Tanaka H., Kiyobayashi T. and Kuriyama N., "Hydrogenation Properties of RNi_5 (R: Rare Earth) Intermetallic Compounds with Multi Pressure Plateaux", *Mater. Trans.*, 2003, 44: 1663.
17. Cullity B. D. and Stock S. R., *Elements of X-Ray Diffraction*, Prentice Hall, 2001:192.
18. Woolfson M. M., *An introduction to X-ray crystallography*, Cambridge University Press, 1997: 113.
19. Srivastava S. and Upadhyaya R. K., "Investigations of AB_5 -type hydrogen storage materials with enhanced hydrogen storage capacity", *Int. J. Hydrogen Energy*, 2012, 36: 7114.
20. Li S. L., Chen W., Luo G., Han X. B., Chen D. M., Yang K. and Chen W. P., "Effect of hydrogen

- absorption/desorption cycling on hydrogen storage properties of a $\text{LaNi}_{3.8}\text{Al}_{1.0}\text{Mn}_{0.2}$ alloy”, *Int. J. Hydrogen Energy*, 2012, 37: 3268.
21. Nakamura Y., Oguro K., Uehara I. and Akiba E., “X-ray diffraction peak broadening and lattice strain in LaNi_5 -based alloys”, *J. Alloys Compd.*, 2000, 298: 138.
22. Nakamura H., Nakamura Y., Fujitani S. and Yonezu I., “Cycle performance of a hydrogen-absorbing $\text{La}_{0.8}\text{Y}_{0.2}\text{Ni}_{4.8}\text{Mn}_{0.2}$ Alloy”, *Int. J. Hydrogen Energy*, 1996, 21: 457.
23. Singh R. K., Lototsky M. V. and Srivastava O. N., “Thermodynamical, structural, hydrogen storage properties and simulation studies of P–C isotherms of $(\text{La,Mm})\text{Ni}_{5-y}\text{Fe}_y$ ”, *Int. J. Hydrogen Energy*, 2007, 32: 2971.
24. Friedlmeier G., Schaaf M. and Groll M., “How to Measure Pressure-Concentration-Isotherms Representative for Technical Applications”, *Z. Phys. Chem.*, 1994, 183: 185.
25. Cocciantelli J. M., Bernard P., Fernandez S. and Atkin J., “The influence of Co and various additives on the performance of $\text{MmNi}_{4.3-x}\text{Mn}_{0.33}\text{Al}_{0.4}\text{Co}_x$ hydrogen storage alloys and Ni/MH prismatic sealed cells”, *J. Alloys Compd.*, 1997, 253–254: 642.
26. Endo D., Sakaki K. and Akiba E., “Formation of lattice strain in $\text{MmNi}_{4.30-x}\text{Co}_x\text{Al}_{0.30}\text{Mn}_{0.40}$ ($x = 0, 0.75$) during hydrogenation”, *J. Alloys Compd.*, 2008, 459: 215.
27. Voskuilen T., Zheng Y. and Pourpoint T., “Development of a Sievert apparatus for characterization of high pressure hydrogen sorption materials”, *Int. J. Hydrogen Energy*, 2010, 35: 103387.
28. Bowman R. C. and Fultz B., “Metallic Hydrides I: Hydrogen Storage and Other Gas-Phase Applications”, *MRS Bull.*, 2002, 27: 688.
29. Zhang T. B., Wang X. F., Hu R., Li J. S., Yang X. W., Xue X. Y. and Fu H. Z., “Hydrogen absorption properties of $\text{Zr}(\text{V}_{1-x}\text{Fe}_x)_2$ intermetallic compounds”, *Int. J. Hydrogen Energy*, 2012, 37: 2328.
30. Mungole M. N. and Balasubramaniam R., “Effect of hydrogen cycling on the hydrogen storage properties of $\text{MmNi}_{4.2}\text{Al}_{0.8}$ ”, *Int. J. Hydrogen Energy*, 2000, 25: 55.
31. Cheng H. H., Yang H. G., Li S. L., Deng X. X., Chen D. M. and Yang K., “Effect of hydrogen absorption/desorption cycling on hydrogen storage performance of $\text{LaNi}_{4.25}\text{Al}_{0.75}$ ”, *J. Alloys Compd.*, 2008, 453: 448.
32. Sandrock G., “A panoramic overview of hydrogen storage alloys from a gas reaction point of view”, *J. Alloys Compd.*, 1999, 293-295: 877.
33. Pourarian F. and Wallace W. E., “The effect of substitution of Mn or Al on the hydrogen sorption characteristics of CeNi_5 ”, *Int. J. Hydrogen Energy*, 1985, 10: 49.
34. An X.H., Gu Q. F., Zhang J. Y., Chen S. L., Yu X. B. and Li Q., “Experimental investigation and thermodynamic reassessment of La-Ni and LaNi_5 -H systems”, *Calphad*, 2013, 40: 48.
35. Da-li C., Hong-hui C., Lei M., De-min C., Man-qi L. and Ke Y., “Effects of Al partial substitution for Ni on properties of $\text{LaNi}_{5-x}\text{Al}_x$ ”, *Trans. Nonferrous Met. Soc. China*, 2007, 17: s967.
36. Zhang X., Li Q. and Chou K-C., “Kinetics of hydrogen absorption in the solid solution region for Laves phase $\text{Ho}_{1-x}\text{Mm}_x\text{Co}_2$ ($x = 0, 0.2$ and 0.4) alloys”, *Intermetallics*, 2008, 16: 1258.
37. Satya Sekhar B., Suresh P. and Muthukumar P., “Performance tests on metal hydride based hydrogen storage devices”, *Int. J. Hydrogen Energy*, 2013, 38: 9570.
38. Muthukumar P., Satheesh A., Linder M., Mertz R. and Groll M., “Studies on hydriding kinetics of some La-based metal hydride alloys”, *Int. J. Hydrogen Energy*, 2009, 34:

7253.

39. Ivey D. G. and Northwood D. O., "Storing energy in metal hydrides: a review of the physical metallurgy", *J. Mater. Sci.*, 1983, 18: 321.

40. An X. H., Pan Y. B., Luo Q., Zhang X., Zhang J.Y. and Li Q., "Application of a new kinetic model for the hydriding kinetics of $\text{LaNi}_{5-x}\text{Al}_x$ ($0 \leq x \leq 1.0$) alloys", *J. Alloys Compd.*, 2010, 506: 63.

41. Ming L., Lavendar E. and Goudy A. J., "The hydriding and dehydriding kinetics of some RCo5 alloys", *Int. J. Hydrogen Energy*, 1997, 22: 63.

42. Johnson W. A. and Mehl R. F., "Reaction kinetics in processes of nucleation and growth", *Trans. Am. Inst. Min. Metall. Eng.*, 1939, 135: 416.

43. Jander W., "Reaktionen im festen Zustande bei höheren Temperaturen. Reaktionsgeschwindigkeiten endotherm verlaufender Umsetzungen", *Z. Anorg. Allg. Chem.*, 1927, 163: 1.

44. Osovizky A., Bloch J., Mintz M. H. and Jacob I., "Kinetics of hydride formation in massive LaNi_3 samples", *J. Alloys Compd.*, 1996, 245: 168.